2019 IEEE/RSJ International Conference on Intelligent Robots and Systems (IROS)
Macau, China, November 4-8, 2019

Experimental Study on Microfluidic Mixing with Trapezoidal Obstacles in a 1000-Fold Span of Reynolds Number*

Xin-Yu Lin[1], Hiroaki Ito[2], Makoto Kaneko[2], Chia-Hung Dylan Tsai[1§]

Abstract— **Mixing is important for microfluidic systems and placing obstacles in a flow path for generating advection, or splitting/recombination flows, is a very popular method for enhancing the mixing. In this paper, we present experimental investigations on such microfluidic mixing with four different shapes of trapezoidal obstacles and tested them in a 1000-fold span of Reynolds number (Re). The obstacles have four different base ratios 1, 3, 6 and 9, which indicate the ratios between the upper and lower bases of a trapezoid. Two different dyes, yellow and blue, were used for visualizing and evaluating the performance of mixing. The results show that, when the base ratio is 1, the mixing surprisingly becomes worse with the increase of the flowrate. When the ratio is 3 or 6, the mixing performance is first reduced with the increase of Re and then went through a transition around Re of 10 before it rapidly increases. When the ratio is 9, two transition points were found around Re of 10 and 100, respectively. The work provides useful information for realizing shape-dependent mixing performance, as well as for developing an intelligent lab-on-a-chip system.**

I. INTRODUCTION

Microfluidic mixing has been widely used in lab-on-a-chip (LOC) applications, such as for sample dilution and solution preparation [1]–[4]. For example, a dilution of blood is necessary for the single-cell evaluation of red blood cells due to the high concentration of the cells in blood [5]. Hellenkamp *et al.* used winding channels for fast and homogeneous diffusion-based mixing with protein complex [6]. Reynolds number (Re) in a microfluidic environment is usually low and it causes difficulties in mixing due to very limited contact surface for diffusion in laminar flow regime. In order to resolve such difficulties, different methods have been developed for enhancing microfluidic mixing in the last two decades [7]. Among the methods, many of them involve multiple designs in one system to increase the mixing performance. For example The *et al*. proposed a mixer combining both trapezoidal cross-section and zigzag channel [8]. Here in this work, we focus on the sole effect of how a trapezoidal obstacle benefits such a microfluidic mixing and the goal is to help LOC developers choose a proper mixer design for their device to build up an intelligent system.

Figure 1 shows an overview of this work. Figure 1(a) includes two experimental results where two different colors, yellow and blue, were mixed by flowing through the same shape of trapezoidal obstacles, from the left to the right, with a 1000-fold difference of Re. One of Re is 0.308 and the other is 308.7. The Re here can be considered as a representation of flow speed since the dimensions of the channel and the fluid properties were identical. For the Re of 0.308 on the left of Figure 1(a), the color layers are parallel to the shape of the channel. A gradient of color from yellow to blue can be seen along vertical lines from the top to the bottom. The color layers can be also seen at the outlet of the chamber, as the zoom-in view in Figure 1(a), and it indicates an imperfect mixing. On the other hand, the result with Re of 308.7 on the right of Figure 1(a) shows a completely different flow pattern. Distorted streamlines and vortices were found inside the chamber which significantly increased the contact surface of the two input colors. As a result, the fluid color was mostly green at the outlet of the chamber and it indicates a good mixing even in a laminar flow regime.

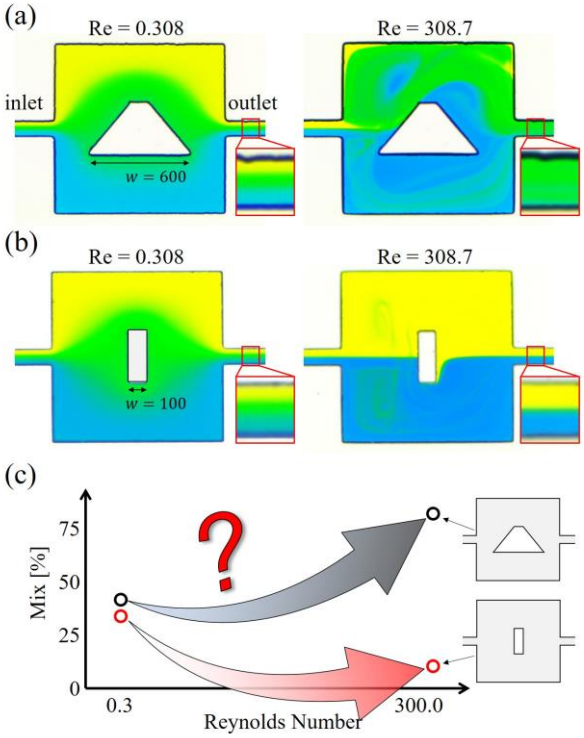

Figure 1. Different characteristics of microfluidic mixing with different trapezoidal obstacles. (a) The mixing performance improves with the increase of Re. (b) The mixing performance reduces with the increase of Re. (c) This study experimentally addresses the anomalous mixing efficiency with respect to a 1000-fold span of Reynolds number with different obstacles.

Figure 1(b) shows the experimental results with a different trapezoidal obstacle whose base ratio is equal to 1, that is, the

*Research is supported by the Taiwan Ministry of Science and Technology 108-2218-E-009-013-, 108-2221-E-009-107- and 108-2321-B-009-004-.
[1]X. Lin and C. D. Tsai are with the Department of Mechanical Engineering, National Chiao Tung University, Taiwan.
[2]H. Ito and M. Kaneko were with the Department of Mechanical Engineering, Osaka University, Japan. Currently, H. Ito is with the Department of Physics, Chiba University, Japan. M. Kaneko is with the Graduate School of Science and Technology, Meijo University, Japan.
§All correspondence should be addressed to Chia-Hung Dylan Tsai (e-mail:dylantsai@nctu.edu.tw)

upper and bottom bases are both 100 μm. The results of mixing in low Re is similar to the one in Figure 1(a), which is not a perfect mixing. When the Re is increased to 308.7, vortices can be seen in the photo, but the mixing response is completely different from the one in Figure 1(a) that the high Re surprisingly results in a worse mixing than the low Re. The results indicate that different shape of trapezoidal obstacle would result in totally different characteristics in terms of mixing. The difference between Figs. 1(a) and (b) motivated this work for revealing the mixing characteristics of different trapezoidal obstacles, as the idea illustrated in Figure 1(c).

The rest of this paper is organized as follows: After a brief review of different microfluidic mixing works in Section II, experimental details are explained in Section III. Experimental results including the raw images of mixing and evaluation of mixing performance are presented in Section IV. Discussions based on the results are in Section V. Finally, the concluding remarks are listed in Section VI.

II. Related Works

Microfluidic mixing is usually categorized into two groups, which are active and passive mixing [4]. Active mixing devices are the ones involving additional driving mechanisms other than a constant flow source. For example, Glasgow and Aubry used peristaltic pumps to create time-pulsing flow to enhance microfluidic mixing [9]. Lu *et al.* fabricated a magnetic microstirrer which can rotate inside a microfluidic channel with a rotating magnetic field, and demonstrate a speed-dependent mixing efficiency [10]. Rezk *et al.* used surface acoustic waves to achieve uniform mixing in paper-based microfluidic systems [11]. On the other hand, passive mixing is the mixing method mostly implemented with geometric designs. Fundamental mechanism for passive mixing includes splitting-recombining, twisting, transversal flows, vortices, and chaotic advection [12]. For example, Kim *et al.* arranged F-shape mixing unit in two layers to achieve splitting-recombination and chaotic advection flows [13]. Stoock *et al*. enhanced mixing using grooves structure at the bottom of the channel [14].

While many studies on microfluidic mixing are based on computational simulation due to complexity in flow control, as well as uncertainties in a dynamic system, an experimental investigation is very important to understand the actual performance of the mixer. In this work, all the results were obtained through actual experiments. A 1000-fold span of Re, from 0.308 to 308.7, for the mixing with trapezoidal obstacle were tested.

III. Experiments

A. Experimental Setup and Flowrates

Figure 2 is an overview of the experimental setup where Figures 2(a) and (b) are photos of the experimental system and the mixing chambers with different trapezoidal obstacles, respectively. The experimental system in Figure 2(a) includes an inverted microscope, a syringe pump a digital complementary metal-oxide semiconductor (CMOS) camera, a computer and a microfluidic chip where trapezoidal obstacles with different base width are. Each microfluidic chip contains all 4 different shapes of trapezoidal obstacles, so the dimensions, such as height and polydimethylsiloxane (PDMS)

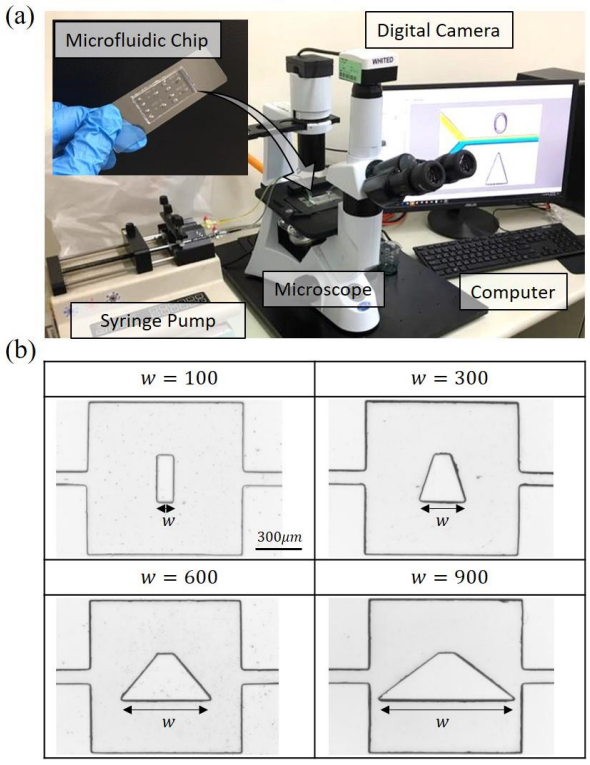

Figure 2. Experimental setup. (a) A photo of experimental system. (b) Photos of fabricated microfluidic mixing chamber with different trapezoidal obstacles.

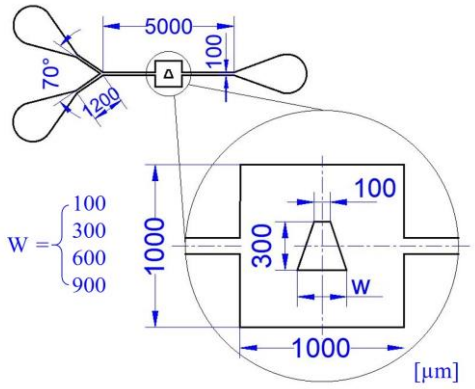

Figure 3. The design and dimensions of channel with trapezoidal obstacle in the mixing chamber.

thickness, of the fabricated mixing channels can be considered similar. The CMOS camera was mounted on the inverted microscope and the digital images were observed and recorded on the computer in realtime. Figure 2(b) shows photos of four different trapezoidal obstacles in mixing chambers. The width of bottom base, *w*, is the only varying dimension in the four designs, and they are w = 100 μm, w = 300 μm, w = 600 μm, and w = 900 μm, respectively.

The syringe pumps with two syringe rack were used for the flow control on both inlets. Teflon tubes were used to connect the syringes on the pump to the inlets on the microfluidic chip. A flow control unit is embedded inside the syringe pump, and it can precisely control the flowrate as user specified. In this

work, 10 different flowrates were applied in the test and they are, from low to high, 0.001 ml/min, 0.004 ml/min, 0.007 ml/min, 0.01 ml/min, 0.04 ml/min, 0.07 ml/min, 0.1 ml/min, 0.4 ml/min, 0.7 ml/min, and 1 ml/min, respectively.

B. Channel Design

Figure 3 shows the detailed dimensions of the mixing channel and chambers. An overview of the design is shown on the top of Figure 3, where two inlets and one outlet are placed on the left and the right of the mixing chamber, respectively. The fluids entering through the two inlets are first joining at a Y-shape junction. The joint flow then passes through the mixing chamber with a trapezoidal obstacle before going to the outlet on the right. The mixing chamber is a 1000 μm by 1000 μm rectangular chamber where a trapezoidal obstacle with designated shape is placed at the center of the chamber. The total length of the channel from the inlets joint to the outlet is 5000 μm while the mixing chamber is 1000 μm wide, which is considered a short distance for microfluidic mixing. An enlarged view of the design of the mixing chamber is shown in Figure 3. The width of the top base and the height of the trapezoidal obstacle is fixed as 100 and 300 μm, respectively. Four different widths, 100 μm, 300 μm, 600 μm and 900 μm, of the bottom base were employed as the actual photos shown in Figure 2. The microfluidic channel is a single layer design and the depth is 100 μm throughout all the design.

C. Chip Fabrication

The microfluidic chip was fabricated using the standard photolithography method, as illustrated in Figure 4. First, a 100 μm SU-8 layer (MicroChem, USA) was spun coated onto a silicon wafer before it was soft baked at 95 °C for 1hr, as illustrated in Figure 4(a). The coated wafer was then exposed to UV light, as shown in Figure 4(b), with a photomask in a mask aligner. The photomask was printed out using a high-resolution printer on a transparent slide and was pasted onto a glass slide before placing into the mask aligner. Figure 4(c) shows the development of the mold after a post-exposure bake at 95 °C for 10 minutes. The wafer was developed in the SU-8 developer solution (MicroChem, USA) for 17 minutes. The developed mold is then placed in a disposable dish and a mixture of PDMS and curing agent was poured onto it. The ratio of the PDMS and curing agent was 10:1. The design on the developed mold was cast by PDMS for replica as shown in Figure 4(d). After vacuum for 1 hour and curing at 90 °C for 1h, the transparent PDMS was cured and could be peeled off from the mold. Figure 4(e) illustrates that the final process of the chip where the cast design was cut off from the whole PDMS chip with a knife, and the inlets and the outlet for tube connection were made by a punch with the diameter of 1.5 mm. The PDMS chip was then bonded to a glass slide using a plasma device. Finally, the microfluidic chip is fabricated as illustrated in Figure 4(g).

D. Reference Color and Mixing Evaluation

This section shows the method of color calibration and mixing evaluation in this work. The color solutions were made by eatable dye (EverStyle) and deionized water with a proportion of 10:1.The densities are experimentally measured as 1.029 g/cm^3 and 1.0288 g/cm^3 for the yellow and blue solutions, respectively. The mixed colors were injected into

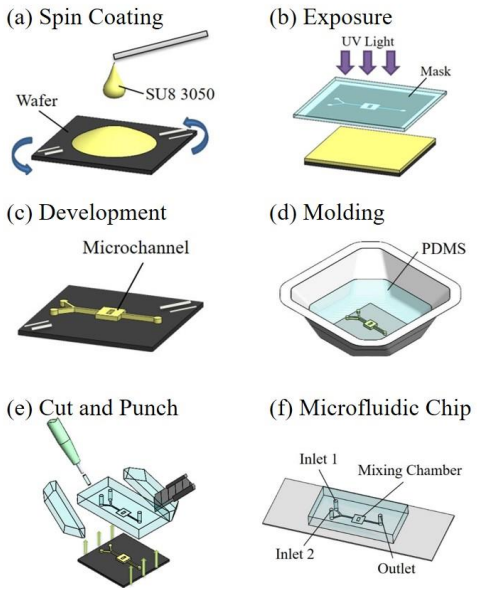

Figure 4. Chip fabrication process. (a) Coat SU-8 on a wafer. (b) Expose to UV light through a mask. (c) Develop the mold. (e) Cast PDMS from the mold. (f) Cut and punch holes on the PDMS chip. (g) Complete the fabrication after bonding to a glass substrate.

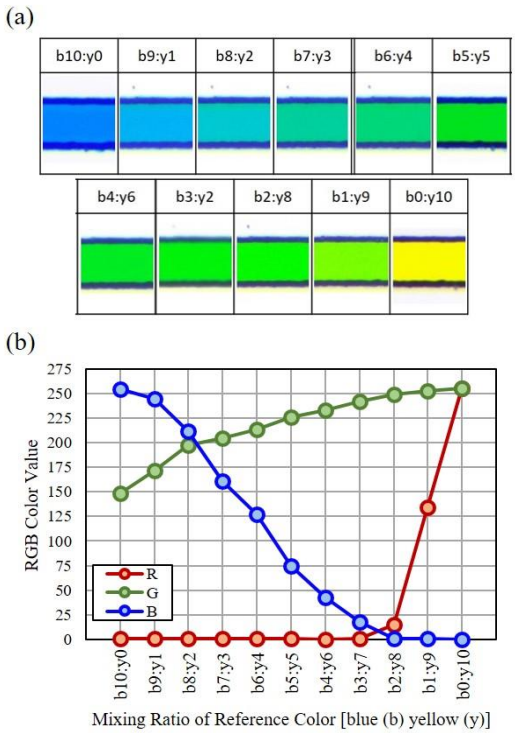

Figure 5. Reference color for mixing evaluation. (a) Photos of the reference colors. (b) RGB values with respect to b:y ratios.

the microchannel, and images were taken using the COMS camera through the microscope. Figure 5(a) shows 11 images of the mixing results with the labels specified the mixing ratios of the two dyes, where the compositions of the blue and yellow dyes are noted in lower-case letters "b" and "y", respectively. For example, "b4:y6" indicates the ratio between the blue and

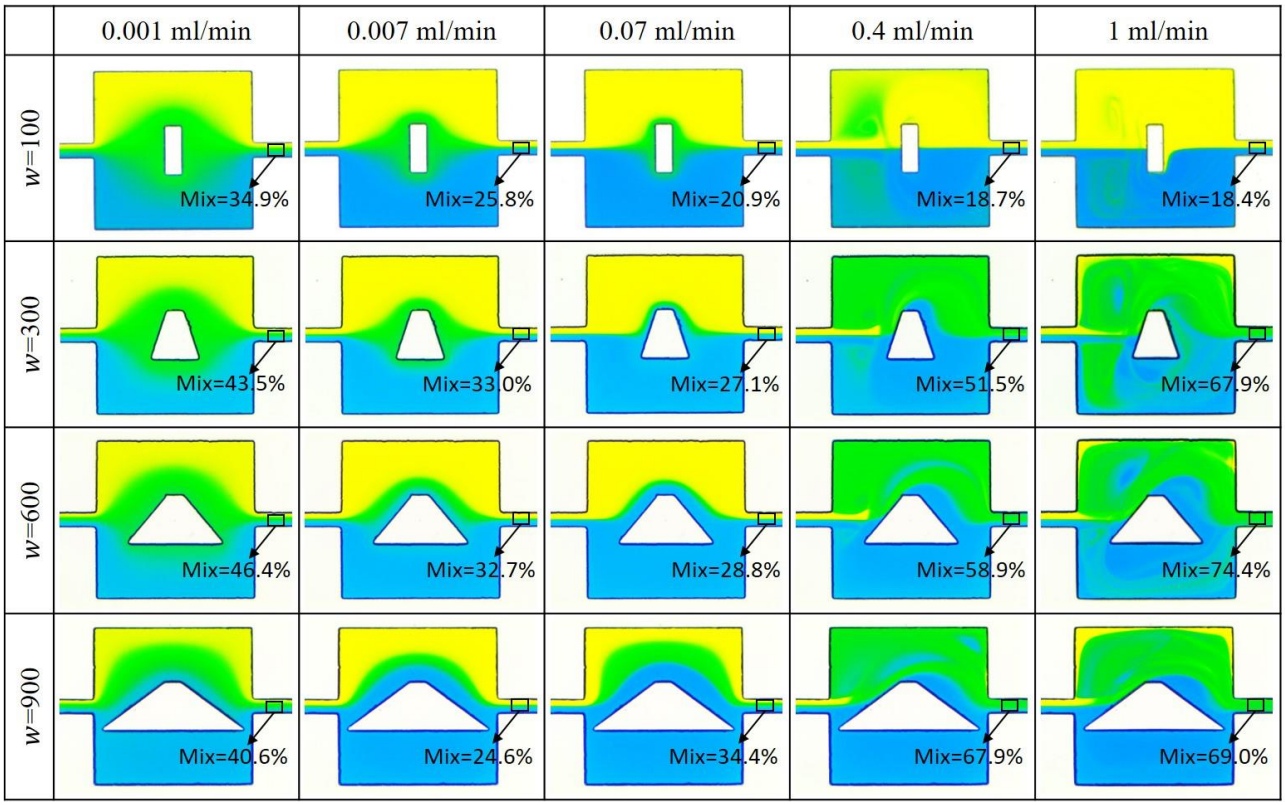

Figure 6. Experimental results with different flowrates and different width. Flowrates of 0.001, 0.007, 0.07, 0.4, 1.0 ml/min, respectively. Widths of 100, 300, 600, 900, respectively.

yellow dyes as 4:6, and the concentration of the yellow dye can be calculated as 60%.

Figure 5(b) shows the evolution of the red, green and blue components with different mixing ratios of the two dyes. The components were extracted from the captured images using the image processing toolbox of MATLAB 2017 (Mathoworks, USA). For the convenience of reading, red, green and blue components are indicated by upper-case letters R, G and B, respectively. According to the results in Figure 5(b), the R values remain zero when the concentration of blue dye is more than 30%. The B values, on the other hand, remain zero when the concentration of blue dye is less than 30%. Only the G value changes with the change of the mixing ratios. That means, either R or B value cannot be solely used to determine the concentration of the two dyes because the values are zeros for a certain range of concentration. Fortunately, G value and the concentration were found in a relation of one-to-one mapping, so that we could choose G value for determining the concentrations of the two dyes. For example, G value of 250 can be mapped to "b1y9" in Figure 5(b) and it represents 10% of blue dye and 90% of yellow dye.

The-least-square algorithm has been applied to perform the curve fit to the G values with respect to the concentration of the yellow dye in Figure 5(b) with an exponential equation

$$G = a\, e^{b\alpha} + c \qquad (1)$$

where G, α, a, b and c are G component of the RGB color, the percentage of yellow dye, and three coefficients, respectively.

TABEL I Fitting Results to G value in Figure 5

Fitting model, Eq.(1)	$G = a\, e^{b\alpha} + c$
Coefficients (a, b, c)	$(-121.3, -1984, 272.1)$
Sum Squared Error (SSE)	80.3233
R Square (R^2)	0.9916
Root Mean Square Error (RMSE)	3.1687

The fit results and the goodness of the fit are shown in Table I. R^2 of the fit is 0.9916 which indicates a good fit as $R^2 = 1$ represents a perfect fit. With Eq. (1) and fit coefficients in Table I, the concentration of yellow dye can be determined from a G value extract from a mixing image.

For evaluating mixing performance, a mixing index is defined as:

$$\text{Mix}\% = 1 - \frac{1}{N}\sum_{i=1}^{N}\sqrt{\left(\frac{\alpha_i - \alpha_{ideal}}{\alpha_{ideal}}\right)^2} \times 100\% \qquad (2)$$

where $\text{Mix}, N, \alpha_i, \alpha_{ideal}$ are the mixing index, the pixel number of the area of interest (AOI), the concentration of the yellow dye from an image, and the concentration of yellow dye of an idea mix, respectively. The ideal concentration α_{ideal} is set 50% since it means 50% of two colors. The defined Mix% is ranged from 0% to 100% where 0% and 100% indicate no mix at all and a perfect mix, respectively.

IV. RESULTS

A. Original Images from the Tests

A total of 10 different flowrates were applied on 4 different trapezoidal obstacles, which give 40 sets of experimental results. For the easiness of reading, Figure 6 shows only the results of 5 different flowrate including 0.001 ml/min, 0.007 ml/min, 0.07 ml/min, 0.4 ml/min, and 1ml/min as representatives. The area of interest and the calculated mixing indices are indicated by black boxes and texts in Figure 6, respectively.

The first row of Figure 6 shows original images with the narrowest bottom width 100 μm, whose base ratio is equal to 1. The mixing performance can be divided into two part with the boundary of the flowrate at 0.07 ml/min. In the first part when the flowrate was in the range of 0.001 ml/min and 0.07 ml/min, the mixing is getting worse with the increase of the flowrate. The performance of the worsened mixing can not only be seen from the calculated mixing indices from the AOI, but also from the color gradient in the mixing chamber. The area of green, the mix of yellow and blue, was greatly reduced with the increasing flowrate. In the second part when the flowrate is greater than 0.07 ml/min, vortices could be visually seen from the images on the left of the mixing chamber. Interestingly, these vortices did not enhance the mixing performance and a consistent reduction of mixing index was obtained from the experiment on the trapezoidal obstacle with w = 100 μm.

The second and the third rows of Figure 6 shows the results with w = 300 μm and w = 600 μm, respectively. These two cases show a similar tendency that the mixing indices were first decreased with the increasing flowrate up to 0.07 ml/min. When the flowrate was beyond 0.07 ml/min, vortices can be visually seen in the mixing chamber due to the trapezoidal obstacles. One clear difference from the results with w = 100 μm is that the mixing performance, as the calculated mixing indices, was greatly enhanced with the apperance of vortices. The mixing indices were double or even triple to the ones without vortices.

The last row of Figure 6 shows the results with w = 900 μm. It also shows a similar tendency that the mixing index was first reduced with the increasing flowrate and then improved afterward. There is still one difference in the result compared with the previous images that the mixing index was improved before being able to visually observe vortices at the flowrate of 0.07 ml/min. To sum up, the mixing performance and tendency with respect to the flowrate were found different under different shapes of trapezoidal obstacles and the flowrates according to the original images shown in Figure 6.

B. Flow Speed Measurement and Reynolds Number

Reynolds number is employed in the analysis for removing dimensional factors from the results. Reynold number, Re, is defined as

$$\mathrm{Re} = \frac{\rho u D}{\mu} \qquad (3)$$

where ρ, u, D, μ are the density of the fluid, the speed of fluid flow, characteristic dimension of the channel, the dynamic viscosity of the fluid. Here we assumed the color solutions having the density and viscosity as $\rho = 10^3\ kg/m^3$, $\mu = 10^{-3}\ N \cdot s\ /m^2$. The characteristic dimension D here is set at $10^{-4}\ m$ as the height of the channel. The remaining term in Eq.(3) is u and here we measured the speed using a high-speed camera and microbeads. Microbeads with a diameter of 1 μm were mixed in the fluid. A total of twelve microbeads at random locations were tracked, and the speeds of microbeads were used to represent the fluid speed. By applying in the average speed into Eq.(3), the Re at the flowrate of 0.001 ml/min is calculated as 0.308, which is about two times greater than the Re estimated using the average speed from the flowrate and cross-sectional area. To avoid underestimating Re in the analysis, the measured flow speed, the greater one, was chosen for the Re estimations.

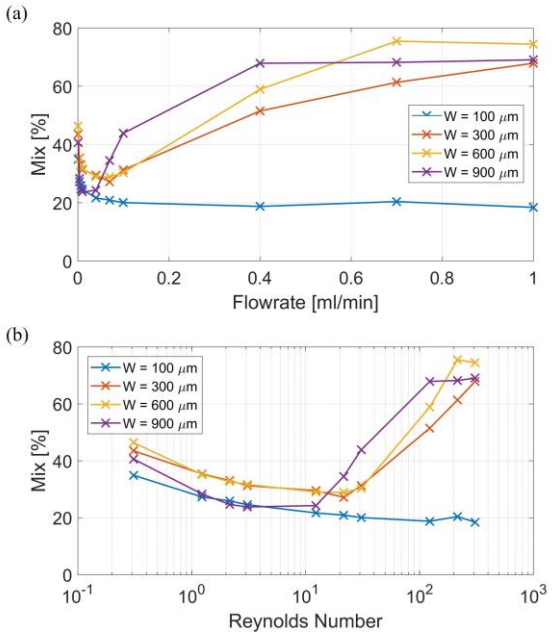

Figure 7. Analysis result of mixing index. (a) Mixing index versus flowrate. (b) Mixing index versus estimated Re where the horizontal axis is in logarithmic scale.

The Re of other flowrates were directly determined from the estimated Re 0.308 at 0.001 ml/min because Re is proportional to the flow speed u, as in Eq. (3). Therefore, the Re for the flowrates of 0.004 ml/min, 0.007 ml/min, 0.01 ml/min, 0.04 ml/min, 0.07 ml/min, 0.1 ml/min, 0.4 ml/min, 0.7 ml/min, and 1 ml/min. are calculated as 1.23, 2.16, 3.08, 12.3, 21.6, 30.8, 123.4, 216.0, 308.6, respectively.

V. DISCUSSION

A. Mixing versus Flowrate / Reynolds Number

Figure 7 shows the analysis results from all images of the 40 sets of test conditions. Figure 7(a) is the relationship between the input flowrate from the syringe pump and the calculated mixing ration with Eq. (2). It can be seen that all trapezoidal obstacles improved the mixing efficiency at flowrates greater than 0.07 ml/min, except the one with w = 100 μm. The mixing performance of the trapezoidal obstacle with w = 100 μm was first rapidly reduced from about 35% to about 20% with respect to the flowrate, and was settled around 18% as there is an asymptotic value. On the other hand,

the trapezoidal obstacles with w = 300, 600, 900 μm were resulting in similar tendency that the mixing performance was first reduced with flowrate and then suddenly improved beyond a transition around 0.07 ml/min flowrate. Among these three designs, the one with w = 600 μm seems to settle at the best mixing performance around 75%.

Figure 7(b) is a different expression of Figure 7(a) with the conversion of flowrates to Re and changing x-axis into a logarithmic scale for better readability on the data points in low Re region. An interesting observation is that the trends of all different trapezoidal obstacles in low Re region are very similar. This indicates that the mixing performance does not depend on the channel design but only on the Re. In other words, the trapezoidal obstacles only effectively affect the mixing performance when Reynolds number is beyond 10.

An interpretation to Figure 7 is that, in the region of Reynolds number less than 10, the mixing effect between two fluids mainly depends on the spontaneous diffusion between two fluids, which is a time-dependent phenomenon according to Fick's laws of diffusion. In other words, a longer mixing time would lead to a better mixing result. Therefore, when the flowrate is getting higher, the mixing time in the mixing chamber would be decreased, which results in the reduced mixing index in Figure 7 at low Re region. When the Re reaches a certain level, which is Re > 10 in this paper, fluids will hit the obstacle due to the inertia and will cause microfluidic vortices in the mixing chamber, where the vortices extend the contact surface of two fluids and improve the mixing.

B. Mixing versus Symmetricity

Another interesting observation from the experiments is the mixing performance of the trapezoidal obstacle with w = 100 μm. It shows a completely different tendency to all other results. The mixing index simply became worse and worse with the increasing flowrate, even when vortices were generated in the mixing chamber as shown in Figure 6. A possible reason is the symmetricity of the obstacle. The trapezoidal obstacle with w = 100 μm is a special case that it is symmetric with respect the centerline along the direction of the channel while all other obstacles are asymmetric. Asymmetricity has been discussed for the mixing in previous study [15]. and we plan to quantify how it benefits the mixing as our future work.

Besides, the increase of the bottom width of the obstacle significantly reduces the chamber area and makes the entrance narrow, which can hinder the flow. To remove such effect, mixing test under a larger proportion of the chamber area will be carried out as another future work.

VI. CONCLUSION

Microfluidic mixing with different trapezoidal obstacles in a mixing chamber has been experimentally investigated under a 1000-fold span of Reynolds number in this work. Three concluding remarks are (1) The shape of obstacle does not significantly affect the mixing when Re < 10. (2) In the region of 10 < Re < 1000, asymmetric obstacles effectively enhanced the mixing but symmetric ones do not. (3) A proper design of passive mixing in a microfluidic device needs to incorporate with its operating Re of the whole system. This work provides experimental insights for the optimization of mixing design in an intelligent LOC system.

REFERENCE

[1] J. Wu *et al.*, "A Passive Mixing Microfluidic Urinary Albumin Chip for Chronic Kidney Disease Assessment," *ACS Sensors*, vol. 3, no. 10, pp. 2191–2197, 2018.

[2] L. Matlock-Colangelo, N. W. Colangelo, C. Fenzl, M. Frey, andA. J. Baeumner, "Passive mixing capabilities of micro-and nanofibres when used in microfluidic systems," *Sensors*, vol. 16, no. 8, pp. 1–18, 2016.

[3] C. Yi, C. W. Li, S. Ji, and M. Yang, "Microfluidics technology for manipulation and analysis of biological cells," *Anal. Chim. Acta*, vol. 560, no. 1–2, pp. 1–23, 2006.

[4] K .Ward and Z. H. Fan, "Mixing in microfluidic devices and enhancement methods," *J. Micromechanics Microengineering*, vol. 25, no. 9, 2015.

[5] C. -H. D. Tsai, S. Sakuma, F. Arai, and M.Kaneko, "A New Dimensionless Index for Evaluating Cell Stiffness-Based Deformability in Microchannel," *IEEE Trans. Biomed. Eng.*, vol. 61, no. 4, pp. 1187–1195, Apr., 2014.

[6] B. Hellenkamp, J. Thurn, M. Stadlmeier, and T. Hugel, "Kinetics of Transient Protein Complexes Determined via Diffusion-Independent Microfluidic Mixing and Fluorescence Stoichiometry," *J. Phys. Chem. B*, p. acs.jpcb.8b07437, 2018.

[7] C. Y. Lee, W. T. Wang, C. C. Liu, and L. M. Fu, "Passive mixers in microfluidic systems: A review," *Chem. Eng. J.*, vol. 288, pp. 146–160, 2016.

[8] H. L. The, B. Q. Ta, H. L. Thanh, T. Dong, T. N. Thoi, and F. Karlsen, "Geometric effects on mixing performance in a novel passive micromixer with trapezoidal-zigzag channels," *J. Micromechanics Microengineering*, vol. 25, no. 9, 2015.

[9] I. Glasgow and N.Aubry, "Enhancement of microfluidic mixing using time pulsing," *Lab Chip*, vol. 3, no. 2, pp. 114–120, 2003.

[10] L. H. Lu, K. S. Ryu, and C. Liu, "A magnetic microstirrer and array for microfluidic mixing," *J. Microelectromechanical Syst.*, vol. 11, no. 5, pp. 462–469, 2002.

[11] A. R. Rezk, A.Qi, J. R. Friend, W. H. Li, and L. Y. Yeo, "Uniform mixing in paper-based microfluidic systems using surface acoustic waves," *Lab Chip*, vol. 12, no. 4, pp. 773–779, 2012.

[12] C. -H. D. Tsai, T. Akai, M. Horade, H. Ito, and M. Kaneko, "Virtual vortex gear," in *Transducers*, pp. 583–586, 2017.

[13] D. S. Kim, S. H. Lee, T. H. Kwon, and C. H. Ahn, "A serpentine laminating micromixer combining splitting/recombination and advection," *Lab Chip*, vol. 5, no. 7, pp. 739–747, 2005.

[14] A. D.Stroock, "Chaotic Mixer for Microchannels," *Science (80-.).*, vol. 295, no. 5555, pp. 647–651, 2002.

[15] J. Li, G. Xia, and Y.Li, "Numerical and experimental analyses of planar asymmetric split-and-recombine micromixer with dislocation sub-channels," *J. Chem. Technol. Biotechnol.*, vol. 88, no. 9, pp. 1757–1765, 2013.